

See discussions, stats, and author profiles for this publication at: <https://www.researchgate.net/publication/263970682>

Electrospun Carbon Nanofibers Decorated with Ag-Pt Bimetallic Nanoparticles for Selective Detection of Dopamine

ARTICLE in ACS APPLIED MATERIALS & INTERFACES · JULY 2014

Impact Factor: 6.72 · DOI: 10.1021/am502344p · Source: PubMed

CITATIONS

19

READS

111

5 AUTHORS, INCLUDING:



[Yunpeng Huang](#)

Fudan University

39 PUBLICATIONS 322 CITATIONS

[SEE PROFILE](#)



[Yue-E Miao](#)

Fudan University

44 PUBLICATIONS 483 CITATIONS

[SEE PROFILE](#)



[Tianxi Liu](#)

Fudan University

233 PUBLICATIONS 6,815 CITATIONS

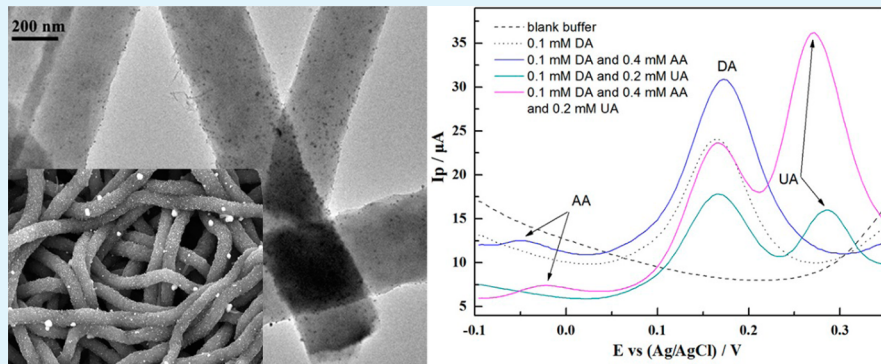
[SEE PROFILE](#)

Electrospun Carbon Nanofibers Decorated with Ag–Pt Bimetallic Nanoparticles for Selective Detection of Dopamine

Yunpeng Huang,[†] Yue-E Miao,[†] Shanshan Ji,[†] Weng Weei Tjiu,[‡] and Tianxi Liu^{*,†}

[†]State Key Laboratory of Molecular Engineering of Polymers, Department of Macromolecular Science, Fudan University, Shanghai 200433, P. R. China

[‡]Institute of Materials Research and Engineering, A*STAR (Agency for Science, Technology and Research), 3 Research Link, Singapore 117602, Singapore



ABSTRACT: Electrospun nanoporous carbon nanofibers (pCNFs) decorated with Ag–Pt bimetallic nanoparticles have been successfully synthesized by combining template carbonization and seed-growth reduction approach. Porous-structured polyacrylonitrile (PAN) nanofibers (pPAN) were first prepared by electrospinning PAN/polyvinylpyrrolidone (PVP) blend solution, followed by subsequent water extraction and heat treatment to obtain pCNFs. Ag–Pt/pCNFs were then obtained by using pCNFs as support for bimetallic nanoparticle loading. Thus, the obtained Ag–Pt/pCNFs were used to modify glassy carbon electrode (GCE) for selective detection of dopamine (DA) in the presence of uric acid (UA) and ascorbic acid (AA). This novel sensor exhibits fast amperometric response and high sensitivity toward DA with a wide linear concentration range of 10–500 μM and a low detection limit of 0.11 μM ($S/N = 3$), wherein the interference of UA and AA can be eliminated effectively.

KEYWORDS: *electrospinning, bimetal, carbon nanofibers, dopamine, detection*

INTRODUCTION

Dopamine (DA), one of the most significant catecholamines that belongs to the family of excitatory chemical neurotransmitters,¹ is extensively distributed in the mammalian central nerve system.² The level of DA in human body has been tied to many disorders like addiction, Parkinson's disease, and schizophrenia,^{3–5} making it play a significant role in human metabolism as well as in the central nervous and renal system. Therefore, DA has been given tremendous attention in biomedical and analytical investigations and there is an urgent necessity to establish a sensitive, selective, and reliable method for the direct detection of DA.

There are many reports about the simultaneous determination of DA, such as fluorescence quenching method,⁶ mass spectrometry,⁷ and capillary electrophoresis.⁸ However, most of these protocols are high-cost, time-consuming, and even relying on special equipment. Electrochemical method otherwise offers itself as an ideal alternative due to its quantitative determination. Recently, electrochemical sensors have been widely studied for DA sensing with the advantages of high

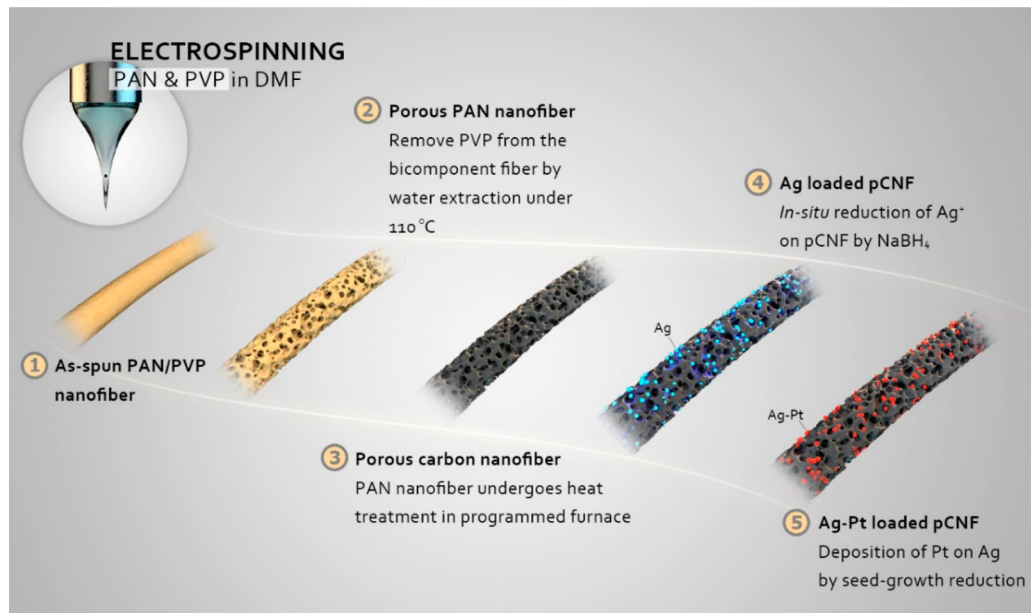
sensitivity, good controllability, and rapid response.^{9,10} However, with a much higher concentration (about 1000 times) than that of DA and similar oxidation potentials to DA,¹¹ coexistence of AA and UA in biological fluids often causes severe interference,¹² which leads to poor selectivity and sensitivity for DA detection. Therefore, it is essential to separate the overlapping signals of DA and AA or UA from each other. To solve this problem, chemically and physically modified electrodes have been widely developed. For example, researchers successfully prepared graphene oxide (GO)-modified GCE for the simultaneous determination of both DA and AA.¹³ Electrospun CeO₂/Au composite nanofibers were investigated as an electrode modifier for the sensitive detection of DA.¹⁴ GCE modified with Pd nanoparticle/graphene/chitosan was also used for the selective determination of AA, DA, and UA.¹⁵ Especially, noble metal nanoparticles

Received: April 17, 2014

Accepted: July 16, 2014

Published: July 16, 2014

Scheme 1. Schematic Illustration of the Preparation of Ag–Pt/pCNFs



have emerged as promising materials in recent years and show inspiring potentials in sensing because of their unusual physical and chemical properties. Among all kinds of noble metals, Pt-nanoparticle-modified electrodes have attracted much attention because of their high surface area, effective mass transport, and high catalytic activity,^{16,17} whereas the low utilization efficiency and high cost of Pt seriously limit its development in commercial applications. An alternative is to introduce a second metal to construct bimetallic structures, which may exhibit fascinating properties different from their corresponding single-component particles.¹⁸ Till now, only few studies have been reported on bimetallic-nanoparticle-modified electrodes for electrochemical determination of DA.^{19,20}

Because of their high mechanical strength, electrical conductivity, and chemical stability, carbon nanofibers (CNFs) have always been used as electrodes in supercapacitors, secondary batteries, low-temperature fuel cells, and sensors.^{21,22} Recent studies even show that CNFs are able to promote the kinetics of electron transfer reaction, minimize electrode surface fouling and enhance electrocatalytic activity.²³ With the rapid development of electrospinning technique, it provides a straightforward and cost-effective way to produce fibers at the nanoscale.^{24–27} Thus, ultrafine and continuous CNFs can be obtained from carbonization of electrospun PAN nanofibers.^{28–30} The as-prepared self-standing nanofibrous CNF membrane possesses superhigh surface area, which could serve as perfect substrate or carrier for impurity doping. Huang et al. has fabricated Pd-loaded CNFs through electrospinning and subsequent thermal treatment.³¹ The Pd/CNF-modified carbon paste electrode showed good performance in the simultaneous determination of DA.

In the present study, a polymer blend of PAN and PVP in DMF was first electrospun, which was then extracted with water to remove PVP component to obtain porous PAN (pPAN) nanofibers. The pPAN nanofibers finally underwent heat treatment to produce nanoporous CNFs (pCNFs). Factors influencing the porous structures of pPAN and pCNFs were also discussed. Subsequently, Ag–Pt bimetallic nanoparticles (Ag–Pt NPs) were immobilized on pCNFs via

versatile seed-growth reduction of H₂PtCl₆·6H₂O and AgNO₃ with NaBH₄ as a reducing agent. The electrochemical activity of Ag–Pt/pCNF-modified GCE was investigated and its selective detection toward DA was performed in the ternary mixture of DA, UA, and AA.

EXPERIMENTAL SECTION

Materials. Polyacrylonitrile (PAN, $M_w = 150\,000 \text{ g mol}^{-1}$) and polyvinylpyrrolidone (PVP, $M_w = 1\,300\,000 \text{ g mol}^{-1}$) were purchased from Sigma-Aldrich. AgNO₃, *N,N*-dimethylformamide (DMF), ethanol, ascorbic acid (AA) and uric acid (UA) were supplied by Shanghai Chemical Reagent Company. H₂PtCl₆·6H₂O and NaBH₄ were commercially obtained from Sinopharm Chemical Reagent Co. Ltd. 0.2 M phosphate buffer solution (PBS) (pH 7.0) was prepared using Na₂HPO₄ and NaH₂PO₄. All aqueous solutions were prepared with doubly distilled water.

Preparation of pCNFs. The bicomponent PAN/PVP nanofibers were first produced through a facile single-nozzle electrospinning.³² Briefly, precursor solution with specific weight ratio of PAN/PVP was prepared by dissolving PAN and PVP in DMF under magnetic stirring over 10 h. The freshly obtained homogeneous polymer solution was sucked into a syringe with a needle having an inner diameter of 0.5 mm. A vertically positioned grounded aluminum board was used as the collector with the distance between the nozzle and the collector set at 15 cm. The operating voltage and feeding speed used here were 21 kV and 2 mm/min, respectively. Generated PAN/PVP fibrous membrane was then vacuum-dried for 24 h before further treatment.

Electrospun PAN/PVP hybrid fibers were then transferred into a 40 mL Teflon stainless-steel autoclave with deionized water (membrane:water = 90:40 mg/mL) and hydrothermally treated under 110 °C for 48 h to selectively remove PVP. The extracted hybrid fibers were washed with water, dehydrated by suction, and then vacuum-dried to obtain nanoporous PAN fibers.

The preoxidation and carbonization of porous PAN fibers were performed in an electric heat-treating furnace. First, the dried pPAN nanofibers were preoxidized in an air atmosphere under 200–250 °C for 1 h with a heating rate of 1 °C/min. Then, samples were heated up to 500–700 °C at a rate of 5 °C/min and carbonized for 2 h under N₂ atmosphere. The as-obtained porous CNFs were kept in a desiccator.

Decoration of Ag–Pt Bimetallic Nanoparticles. The immobilization of Ag–Pt bimetallic nanoparticles onto pCNFs was conducted by a versatile seed-growth reduction, as shown in Scheme 1. In a typical process, a piece of self-standing pCNF membrane (22.2 mg)

was immersed into a AgNO_3 aqueous solution (10 mM, 20 mL) for 3 h to allow the interaction between Ag^+ ions and pCNF surface. pCNF membrane was then withdrawn from the Ag^+ solution and dropwise added freshly prepared NaBH_4 solution (100 mM, 10 mL) to reduce Ag^+ for 30 min until there was no gas releasing. The as-obtained Ag/pCNFs membrane was rinsed for 3 times with water, followed by drying at 50 °C. Then, the self-standing Ag/pCNF membrane was dipped into a $\text{H}_2\text{PtCl}_6 \cdot 6\text{H}_2\text{O}$ aqueous solution (4 mM, 20 mL) for 1 h to allow the partial replacement of Ag with Pt, which was then rinsed for 3 times with water and dried at 50 °C. Ag–Pt/pCNFs were synthesized from varied Ag^+ concentrations, wherein $c(\text{AgNO}_3)$: $c(\text{H}_2\text{PtCl}_6)$ was kept at 5:2. For comparison, Pt/pCNFs with the same Pt content as Ag–Pt/pCNFs were also synthesized using the above method.

Preparation of Ag–Pt/pCNFs Modified GCE. Before the surface modification, GCE was polished with 1.0, 0.3, and 0.05 μm alumina slurries sequentially, and then ultrasonicated in a mixed solution of deionized water and ethanol (weight ratio = 1:1) for 15 min. Afterward, the electrode was left to dry at room temperature in a desiccator. The Ag–Pt/pCNF membrane was ground to powder before use. For all electrochemical tests, Ag–Pt/pCNF composite modified electrode (denoted as Ag–Pt/pCNFs/GCE) was prepared by 5 μL of 1 mg/mL Ag–Pt/pCNFs powder suspension dropped on the surface of the pretreated GCE and left to dry at room temperature. A similar procedure was applied to prepare the Ag/pCNF-modified electrode (Ag/pCNFs/GCE) and Pt/pCNFs modified electrode (Pt/pCNFs/GCE) for comparison.

Characterization and Electrochemical Measurements. The morphology of samples was investigated using field-emission scanning electron microscope (FESEM, Zeiss) at an acceleration voltage of 5 kV. All samples were coated with a thin layer of gold prior to FESEM observations. TEM observations were performed under an acceleration voltage of 200 kV with a JEOL JEM2100 TEM coupled with an energy-dispersive X-ray (EDX) detector. X-ray diffraction (XRD) experiments were conducted at $2\theta = 10\text{--}80^\circ$ on an X'Pert Pro X-ray diffractometer with $\text{CuK}\alpha$ radiation ($\lambda = 0.1542 \text{ nm}$) under a voltage of 40 kV and a current of 40 mA. All electrochemical measurements were performed using a CHI 660D electrochemical workstation (Shanghai Chenhua Instrument Co., China). A conventional three-electrode system was used, which consists of a modified electrode as the working electrode, a platinum wire as the auxiliary electrode, and an Ag/AgCl (3 M KCl) electrode as the reference electrode. All working solutions were purged with nitrogen for 30 min before measurements. All the electrochemical measurements were performed at room temperature.

RESULTS AND DISCUSSION

Morphology and Structure of Ag–Pt/pCNFs. For the preparation of PAN/PVP hybrid nanofibers, two different compositions of electrospun precursor solutions are investigated, i.e., PAN/PVP/DMF = 6/6/10 and 6/12/10 (g/g/mL). The morphology of electrospun PAN/PVP nanofibers before and after water extraction was characterized by FESEM. As shown in images a and b in Figure 1, nanofibers with different precursor composition are nearly identical in morphology, with smooth and uniform PAN/PVP nanofibers in random orientation exhibiting a mean diameter of about 370 nm. After selective removal of PVP from the hybrid fibers by water treatment, the surface morphology of PAN undergoes tremendous change. As shown in images c and d in Figure 1, distinct porous structures can be observed with the nanopores densely distributed throughout the fibers. It is worth noting that the porous ultrafine PAN nanofibers obtained from water extraction still maintain a continuous and uniform fiber structure. Moreover, the pore size and density are largely enhanced after increasing the PVP content in the hybrid nanofibers. It can be speculated that the formation of the dense

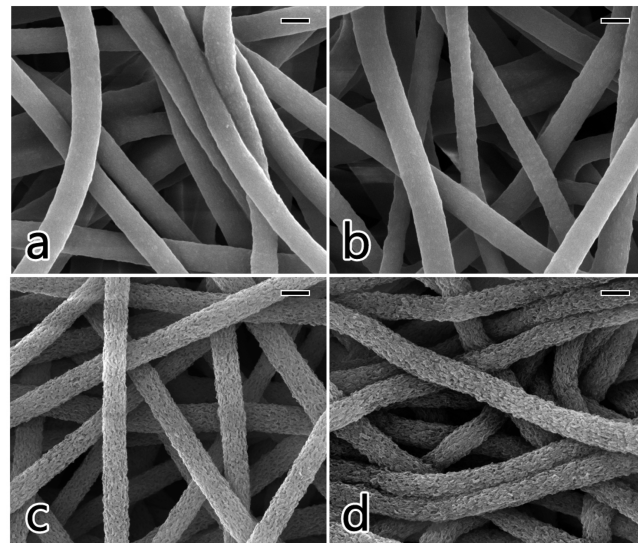


Figure 1. FESEM images of (a, b) electrospun PAN/PVP nanofibers with different compositions and (c, d) corresponding porous PAN nanofibers after water treatment: (a, c) PAN/PVP/DMF = 6/6/10 (g/g/mL); (b, d) PAN/PVP/DMF = 6/12/10 (g/g/mL). Scale bar: 400 nm.

pores on PAN is totally originated from the phase separation of PVP domains during water treatment.

The heat treatment of porous PAN fibers involves two processes of preoxidation and carbonization.³³ During the preoxidation in air at 200–250 °C, PAN undergoes cyclization and partial dehydrogenation which makes it denser and more stable to retain its fibrous structure during subsequent high temperature carbonization. During the carbonization stage at a higher temperature, polymers begin to pyrolyze and a considerable amount of volatile byproducts are released. In our current study, different temperatures in both heat treatment stages are discussed. Figure 2 shows the SEM images of preoxidized and carbonized nanofibers treated at different temperatures. As can be seen (Figure 2a–c), compared to the untreated PAN fibers, different oxidation temperatures lead to the pretty same surface morphology with substantial pores and holes on the fiber surface, although the porous structures are deteriorated to some extent. The above oxidized nanofibers are then carbonized at 500 °C, with Figure 2d–f displaying a very interesting contrast that only the fibers oxidized at 250 °C retain their porous structures while those of the other two oxidized at 200 and 220 °C are completely lost. It can be seen that the surface of fibers oxidized at 200 and 220 °C is quite smooth, with most of the fibers fusing with each other. This is because cyclization and dehydrogenation reaction in the preoxidation process cannot be performed under the relatively lower temperature, which makes the fibers less stable during the high temperature stage. Moreover, fibers preoxidized at 250 °C are also carbonized at three different temperatures. Differences can be observed from Figure 2g–i that fiber diameters significantly decrease compared with that of fibers before heat treatment, which might be caused by the heat-induced contraction. In addition, pore structures of fibers carbonized at 700 °C are superior to those of fibers treated at 500 and 600 °C. As clearly shown in Figure 2j, nanosized pores are not only distributed along the fiber surface, they also exist inside the fibers (as marked by red circles). It is obvious that fibers with

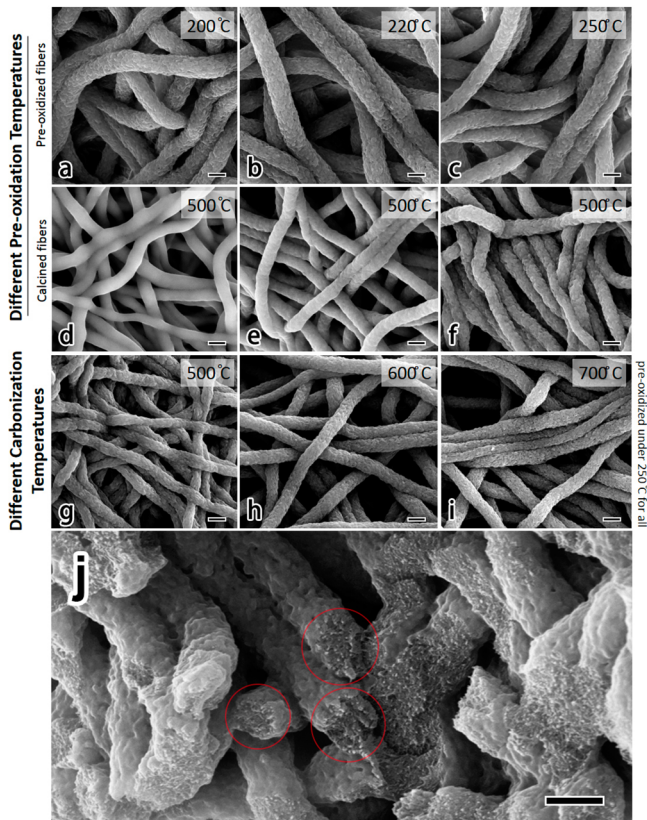
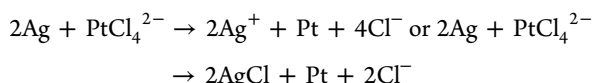


Figure 2. FESEM images of porous PAN nanofibers treated at varied temperatures in (a–f) preoxidation and (g–i) carbonization processes. Cross-sectional image of PAN nanofibers carbonized at 700 °C (j). Scale bar: 400 nm.

more porous structures hold relatively larger specific surface area, making them more suitable as electro-catalyst materials.

In the synthesis of Ag–Pt/pCNFs, Ag nanoparticles were prior decorated on pCNFs to serve as seeds for the subsequent Pt replacement. Therefore, immobilization of the Ag seeds was carefully tuned by varying the Ag^+ concentration in order to obtain an optimized distribution of bimetallic nanoparticles. The ratio of $c(\text{AgNO}_3)$: $c(\text{H}_2\text{PtCl}_6)$ and Pt replacement time were respectively kept at 5:2 and 1 h, according to a procedure reported in the literature but with some modifications.³⁴ The replacement mechanism can be described in the following equation



As displayed in Figure 3, it is clear that the composite fibers still retain nanoporous surface, similar to fibers before treatment. Compared to pCNFs treated in lower Ag^+ concentrations, those treated in 10 mM result in a denser and uniform Ag NP loading, whereas the distributions in images a and b in Figure 3 are obviously sparser. It is notable that there exists a small amount of larger Ag particles on the pCNFs (Figure 3c), which might be caused by the local aggregation during the addition of NaBH_4 . When further increasing the Ag^+ concentration, agglomerated Ag NPs with various sizes are observed on the pCNFs (Figure 3d), which will block the interaction between analytes and pCNF surfaces. As a result, Ag/pCNFs synthesized from 10 mM Ag^+ were used as template for

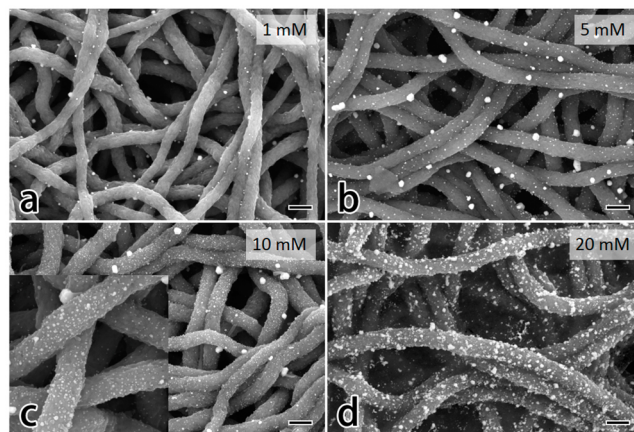


Figure 3. (a–d) FESEM images of Ag/pCNFs synthesized from AgNO_3 solution at varied concentrations. Scale bar: 400 nm.

further loading of Pt nanoparticles. From the TEM images in Figure 4, we can see that the rough surfaces of CNFs are

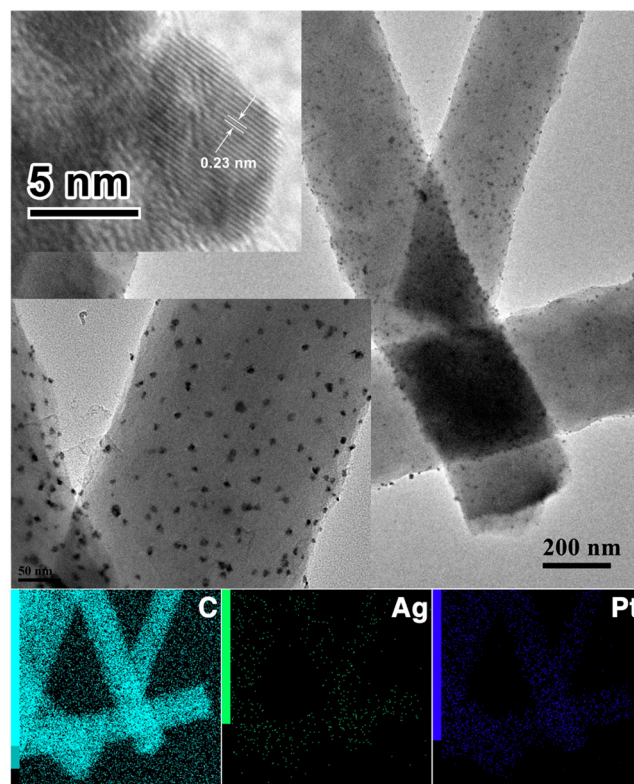


Figure 4. TEM images of Ag–Pt/pCNFs and the corresponding elemental mappings. Inset: high-resolution TEM of Ag–Pt bimetallic nanoparticle.

uniformly covered by Ag–Pt bimetallic nanoparticles with an average size of 6 nm. The corresponding elemental mapping further confirms the existence of the hybrid nanoparticles. The lattice fringes (inset of Figure 4) with interplanar spacing of 0.23 nm correspond to the mean value of the (111) planes of the face-centered cubic (fcc) Ag and Pt, indicating that (111) is the main exposed facet, and Ag–Pt can be initially identified as a metal alloy of Ag and Pt atoms.³⁵

The composition and crystal structure of Ag–Pt/pCNF composite nanofibers were characterized by XRD (Figure 5).

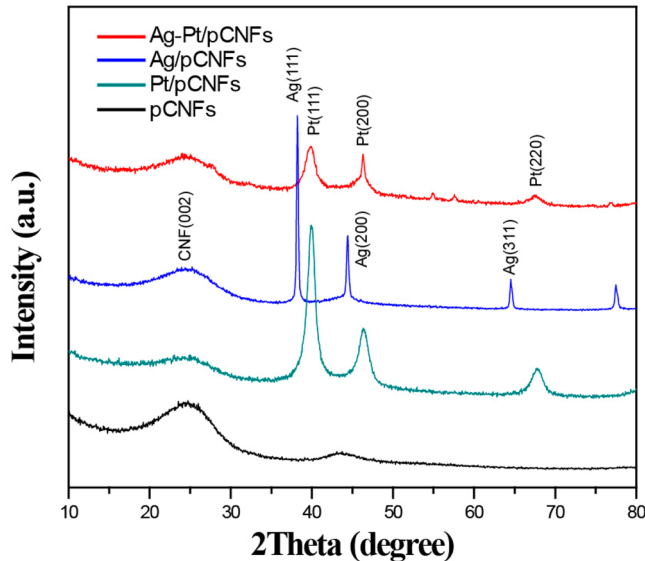


Figure 5. XRD patterns of pCNFs.

The peak located at about $2\theta = 25.0^\circ$ in all of the XRD patterns is associated with the amorphous structure of pCNFs. The diffractions of Ag/pCNFs match well with the characteristic peaks of Ag (i.e., $2\theta = 38.1, 44.2$, and 64.4°) (PDF card 87–0597). In the curve of Pt/pCNFs, the three peaks at 2θ values of $39.8, 46.2$, and 67.4° are characteristic peaks of the face-centered cubic (fcc) crystalline alloys of Pt (PDF card 04–0802), corresponding to the planes of (111), (200), and (220), respectively. In contrast, the Ag signals in the diffraction of Ag–Pt/pCNFs completely vanishes, which indicates that the Ag surface in Ag–Pt is mostly wrapped by Pt.

Electrochemical Determination of DA. To evaluate the electrochemical behavior of different electrodes on the oxidation of DA, we constructed enzymeless DA sensors by direct deposition of the aqueous dispersion of different pCNFs on bare GCE surfaces. Figure 6 shows cyclic voltammetric responses of 0.1 mM DA in 0.1 M PBS (pH 7) on different pCNFs modified GCE. No obvious redox peaks can be observed on Ag–Pt/pCNFs/GCE in blank PBS from the inset

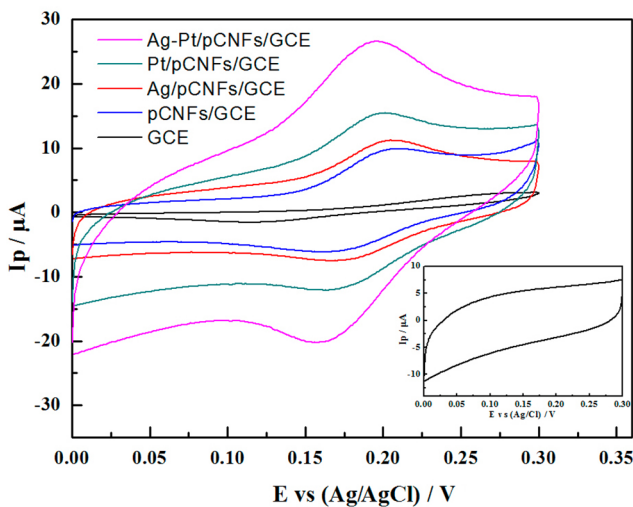


Figure 6. CV curves of modified GCE in the presence of 0.1 mM DA in pH 7.0, 0.1 M N_2 saturated PBS. Scan rate: 50 mV/s . Inset: CV curve of Ag–Pt/pCNFs/GCE in blank PBS.

of Figure 6, indicating that Ag–Pt/pCNFs/GCE is stable in the selected potential region without any redox reaction. In DA solution, a pair of redox peaks appears on the modified GCE with the increase in the voltammetric responses, which is due to the modification of electrocatalytic decorated pCNFs. The results indicate that the electro-oxidation of DA occurred and was accelerated by the step-by-step modification of GCE. From the CV curves, we can see DA exhibits noticeable electrochemical response on pCNFs/GCE, which is contributed to the presence of nanoporous, large surface area and conductive pCNFs. With Ag/pCNFs on GCE, the DA voltammetric response increases somewhat due to the catalytic Ag loading. Moreover, Pt/pCNFs/GCE further improves the anodic peak current of DA compared to Ag/pCNFs/GCE, which is ascribed to the high catalytic property of Pt. In the case of Ag–Pt/pCNFs/GCE, a well-defined oxidation peak of DA is observed at about 0.196 V vs Ag/AgCl , exhibiting the largest redox peak currents than the other modified GCE. Compared with their corresponding monometallic nanoparticles, the superior electrocatalytic performance of Ag–Pt bimetallic nanoparticles is caused by the modification of electronic properties and synergistic effect at the interface of Ag–Pt binary structure.³⁶ The above results suggest that Ag–Pt/pCNF nanocomposite on the GCE has greatly improved the electrocatalytic ability toward DA oxidation.

To better understand the electrochemical mechanism of DA on Ag–Pt/pCNFs/GCE, electrochemical parameters of DA on the modified electrode are further investigated. The effect of different scan rates on the cyclic voltammetric response of 0.1 M DA on Ag–Pt/pCNFs/GCE is shown in Figure 7. With the

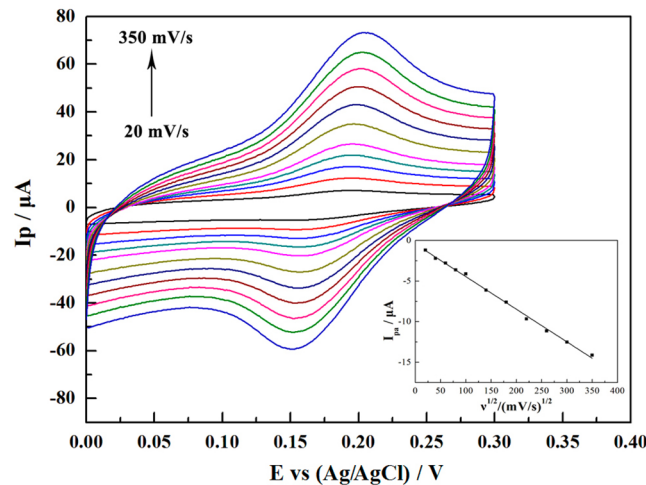


Figure 7. CV curves of 0.1 mM DA on Ag–Pt/pCNFs/GCE with different scan rates ($20, 40, 60, 80, 100, 140, 180, 220, 260, 300, 350 \text{ mV/s}$) in pH 7.0, 0.1 M N_2 saturated PBS. Inset: linear relationship of the anodic peak current with the square root of the scan rate.

increase of scan rate from 20 mV/s to 350 mV/s , the redox peak current increases gradually with a pair of symmetric redox peaks appeared. The inset of Figure 7 presents the calibration curve of the response peak current to the square root of different scan rates. The linear response range is obtained from 20 to 350 mV/s and the linear regression equation is $I (\mu\text{A}) = -0.0402v^{1/2} (\text{mV/s})^{1/2} - 0.4416 (R^2 = 0.997)$, where I and v represent peak current and scan rate, respectively. This manifests that the redox process of DA at Ag–Pt/pCNFs/GCE is a diffusion-controlled process.

Figure 8 displays the typical differential pulse voltammetry (DPV) curves corresponding to the electrocatalytic oxidation of

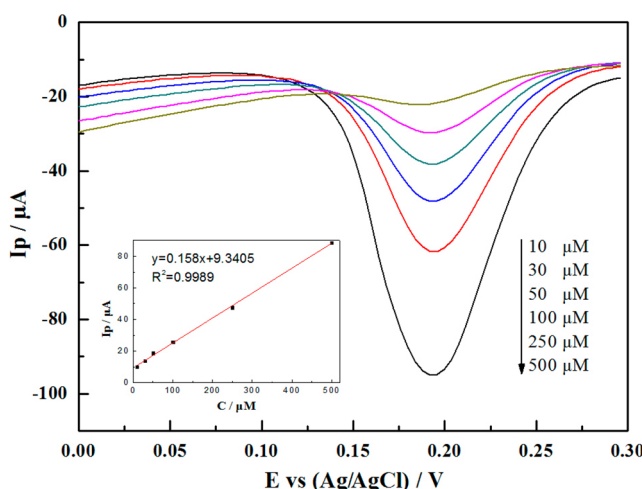


Figure 8. DPV curves of different concentrations of DA (10, 30, 50, 100, 250, 500 μM) on Ag–Pt/pCNFs/GCE in 0.1 M N_2 saturated PBS. Inset is the linear relationship between the peak current and DA concentration.

DA at Ag–Pt/pCNFs/GCE in N_2 saturated PBS at the scan rate of 50 mV/s. As shown in Figure 8, upon increasing the concentration of DA in PBS, the oxidation peak current exhibits remarkable enhancement, which suggests that Ag–Pt/pCNFs/GCE could be applied to the quantitative determination of DA. The anodic peak current (I_{pa}) of DA has a good linear relationship with DA concentration in the range from 10 to 500 μM (inset of Figure 8). The linear regression equation is I (μA) = $0.158c$ (μM) + 9.341 ($R^2 = 0.9989$), where I and c represent anodic peak current and DA concentration, respectively. The limit of detection is found to be 0.11 μM ($S/N = 3$), which is better than some previous reports (shown in Table 1). It is evident that this Ag–Pt/pCNFs/GCE has excellent electrochemical activity and can be a promising sensor for DA determination.

UA and AA always exist in biological environment along with DA, so the simultaneous determination of DA in the presence of UA and AA is significantly important. The influence of UA and AA on the determination of 0.1 mM DA was conducted by

Table 1. Comparison of Some Characteristics of Different Novel Metal-Based Electrodes for the Determination of DA

electrode	electrolyte	detection limit (μM)	linear range (μM)	refs
RGO/Pd-NPs/GCE	pH 7	0.233	1–150	37
Au-NPs/PANI/GCE	pH 4	0.8	3–115	38
Pd/CNF/CPE ^a	pH 7	0.2	0.5–160	31
Au/PE/PS/BDD ^b	pH 7.2	0.8	5–100	39
PANI/Au/nanoelectrode	pH 6.8	0.1	0.3–200	40
Ag–Pt/pCNFs/GCE	pH 7	0.11	10–500	this work

^aCarbon paste electrode. ^bGold nanoparticles and polyelectrolyte (PE) on polystyrene (PS)-modified boron-doped diamond (BDD) electrode.

adding one or two of them in the DA buffer solution and measuring the electrochemical responses by DPV, as shown in Figure 9. From the results we can see upon the addition of UA

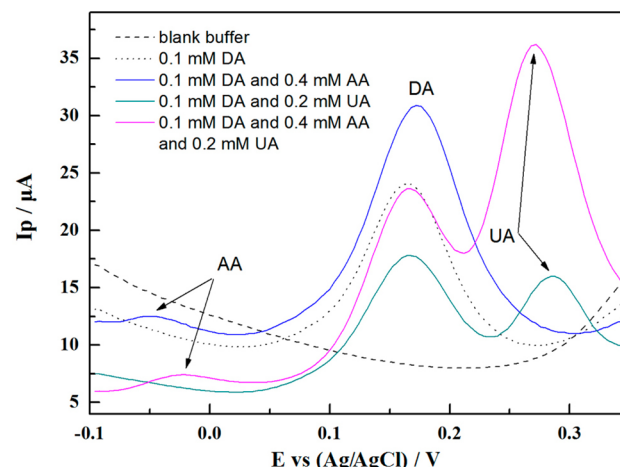


Figure 9. DPV curves of 0.1 mM DA and/or other interference (0.2 mM UA and/or 0.4 mM AA) on Ag–Pt/pCNFs/GCE.

or AA, well-defined two oxidation peaks can be observed, indicating that UA or AA alone cannot influence the sensitive detection of DA. When both of them are involved for the electrochemical detection of DA, still no interference is observed for the excess addition of UA and AA, which reveals that this Ag–Pt/pCNFs/GCE has excellent selectivity to DA determination.

The stability of the Ag–Pt/pCNF nanocomposite-modified GCE was investigated by measuring the current response to 0.1 mM DA for 300 cycles in PBS. As shown in Figure 10, the response current of Ag–Pt/pCNFs/GCE to DA almost maintains 80% of the initial value after 300 rounds of cyclic scanning, indicating good stability.

CONCLUSION

A novel DA sensor has been fabricated by template carbonization of water-extracted electrospun PANI nanofibers, followed by seed-growth reduction to realize the immobiliza-

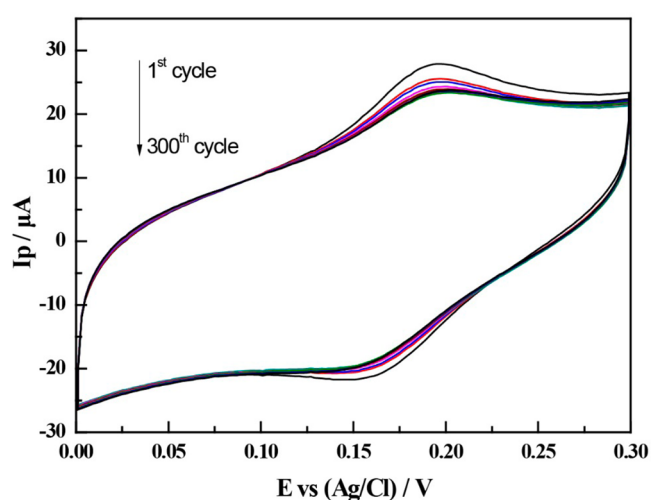


Figure 10. Stability tests of Ag–Pt/pCNFs/GCE in the presence of 0.1 mM DA in pH 7.0, 0.1 M N_2 saturated PBS. Scan rate: 50 mV/s.

tion of Ag–Pt bimetallic nanoparticles. Thus, the prepared Ag–Pt/pCNFs were utilized for modification of GCE to selectively detect DA in the presence of UA and AA. In this work, parameters influencing the porous structure of CNFs and distribution of Ag–Pt nanoparticles are carefully investigated. Compared with their corresponding monometallic nanoparticles, Ag–Pt/pCNFs decorated GCE exhibit superior electrocatalytic performance due to the synergistic effect at the interface of Ag–Pt binary structure. The proposed Ag–Pt/pCNFs/GCE shows advantages including high sensitivity, wide linear range of 10–500 μM, low detection limit of 0.11 μM ($S/N = 3$), and excellent selectivity under the interference of UA and AA. These characteristics suggest that electrospun nanoporous CNFs are an excellent substrate for the Ag–Pt NPs loading with high electrocatalytic activity toward DA.

AUTHOR INFORMATION

Corresponding Author

*E-mail: txliu@fudan.edu.cn. Tel: +86-21-55664197. Fax: +86-21-65640293.

Notes

The authors declare no competing financial interest.

ACKNOWLEDGMENTS

The authors are grateful for the financial support from the National Natural Science Foundation of China (51373037, 51125011).

REFERENCES

- (1) Wightman, R. M.; May, L. J.; Michael, A. C. Detection of Dopamine Dynamics in the Brain. *Anal. Chem.* **1988**, *60*, 769A–793A.
- (2) de Araujo, I. E.; Ferreira, J. G.; Tellez, L. A.; Ren, X.; Yeckel, C. W. The Gut-Brain Dopamine Axis: A Regulatory System for Caloric Intake. *Physiol. Behav.* **2012**, *106*, 394–399.
- (3) Gorwood, P.; Strat, Y.; Ramoz, N.; Dubertret, C.; Moalic, J.; Simonneau, M. Genetics of Dopamine Receptors and Drug Addiction. *Hum. Genet.* **2012**, *131*, 803–822.
- (4) Grace, A. A. Dopamine System Dysregulation by the Hippocampus: Implications for the Pathophysiology and Treatment of Schizophrenia. *Neuropharmacology* **2012**, *62*, 1342–1348.
- (5) Darbin, O. The Aging Striatal Dopamine Function. *Parkinsonism Relat. Disord.* **2012**, *18*, 426–432.
- (6) Wang, H. Y.; Feng, X. G.; Zhang, M.; Zhao, H. Determination of Dopamine in Injections and Urine by an Enzyme-Catalyzed Fluorescence Quenching Method. *Anal. Sci.* **2007**, *23*, 1297–1300.
- (7) Kim, H. R.; Kim, T.; Hong, S.; Kim, H. Direct Detection of Tetrahydrobiopterin (BH_4) and Dopamine in Rat Brain Using Liquid Chromatography Coupled Electrospray Tandem Mass Spectrometry. *Biochem. Biophys. Res. Commun.* **2012**, *419*, 632–637.
- (8) Habibi, B.; Jahanbakhshi, M.; Pouraghazi-Azar, M. H. Simultaneous Determination of Acetaminophen and Dopamine Using SWCNT Modified Carbon-Ceramic Electrode by Differential Pulse Voltammetry. *Electrochim. Acta* **2011**, *56*, 2888–2894.
- (9) Xue, C.; Han, Q.; Wang, Y.; Wu, J. H.; Wen, T. T.; Wang, R. Y.; Hong, J. L.; Zhou, X. M.; Jiang, H. J. Amperometric Detection of Dopamine in Human Serum by Electrochemical Sensor Based on Gold Nanoparticles Doped Molecularly Imprinted Polymers. *Biosens. Bioelectron.* **2013**, *49*, 199–203.
- (10) Zhu, Z.; Qu, L.; Guo, Y.; Zeng, Y.; Sun, W.; Huang, X. Electrochemical Detection of Dopamine on a Ni/Al Layered Double Hydroxide Modified Carbon Ionic Liquid Electrode. *Sens. Actuators, B* **2010**, *151*, 146–152.
- (11) Tang, C.; Kumar, S. A.; Chen, S. Zinc Oxide/Redox Mediator Composite Films-Based Sensor for Electrochemical Detection of Important Biomolecules. *Anal. Biochem.* **2008**, *380*, 174–183.
- (12) Gao, Z.; Huang, H. Simultaneous Determination of Dopamine, Uric Acid and Ascorbic Acid at an Ultrathin Film Modified Gold Electrode. *Chem. Commun.* **1998**, 2107–2108.
- (13) Gao, F.; Cai, X. L.; Wang, X.; Gao, C.; Liu, S. L.; Gao, F.; Wang, Q. X. Highly Sensitive and Selective Detection of Dopamine in the Presence of Ascorbic Acid at Graphene Oxide Modified Electrode. *Sens. Actuators, B* **2013**, *186*, 380–387.
- (14) Tong, Y.; Li, Z. C.; Lu, X. F.; Yang, L.; Sun, W. N.; Nie, G. D.; Wang, Z. J.; Wang, C. Electrochemical Determination of Dopamine Based on Electrospun CeO_2/Au Composite Nanofibers. *Electrochim. Acta* **2013**, *95*, 12–17.
- (15) Wang, X.; Wu, M.; Tang, W. R.; Zhu, Y.; Wang, L. W.; Wang, Q. J.; He, P. G.; Fang, Y. Z. Simultaneous Electrochemical Determination of Ascorbic Acid, Dopamine and Uric Acid Using a Palladium Nanoparticle/Graphene/Chitosan Modified Electrode. *J. Electroanal. Chem.* **2013**, *695*, 10–16.
- (16) Dursun, Z.; Gelmez, B. Simultaneous Determination of Ascorbic Acid, Dopamine and Uric Acid at Pt Nanoparticles Decorated Multiwall Carbon Nanotubes Modified GCE. *Electroanalysis* **2010**, *22*, 1106–1114.
- (17) Mahshid, S.; Li, C. C.; Mahshid, S. S.; Askari, M.; Dolati, A.; Yang, L. X.; Luo, S. L.; Cai, Q. Y. Sensitive Determination of Dopamine in the Presence of Uric Acid and Ascorbic Acid Using TiO_2 Nanotubes Modified with Pd, Pt and Au Nanoparticles. *Analyst* **2011**, *136*, 2322–2329.
- (18) Sun, S.; Murray, C. B.; Weller, D.; Folks, L.; Moser, A. Monodisperse FePt Nanoparticles and Ferromagnetic FePt Nano-crystal Superlattices. *Science* **2000**, *287*, 1989–1992.
- (19) Bai, Y. C.; Zhang, W. D. Highly Sensitive and Selective Determination of Dopamine in the Presence of Ascorbic Acid Using $Pt@Au/MWNTs$ Modified Electrode. *Electroanalysis* **2010**, *22*, 237–243.
- (20) Thiagarajan, S.; Chen, S. M. Preparation and Characterization of PtAu Hybrid Film Modified Electrodes and Their Use in Simultaneous Determination of Dopamine, Ascorbic Acid and Uric Acid. *Talanta* **2007**, *74*, 212–222.
- (21) Joh, H.; Ha, H. Y.; Prabhuram, J.; Jo, S. M.; Moon, S. H. Synthesis of Branched Carbon Nanotubes by Carbonization of Solid Polyvinylidene Fluoride Fibers. *Carbon* **2011**, *49*, 4601–4603.
- (22) Mao, X. W.; Yang, X. Q.; Rutledge, G. C.; Hatton, T. A. Ultra-Wide-Range Electrochemical Sensing Using Continuous Electrospun Carbon Nanofibers with High Densities of States. *ACS Appl. Mater. Interfaces* **2014**, *6*, 3394–3405.
- (23) Wu, L.; Zhang, X.; Ju, H. Detection of NADH and Ethanol Based on Catalytic Activity of Soluble Carbon Nanofiber with Low Overpotential. *Anal. Chem.* **2006**, *79*, 453–458.
- (24) Greiner, A.; Wendorff, J. H. Electrospinning: A Fascinating Method for the Preparation of Ultrathin Fibers. *Angew. Chem., Int. Ed.* **2007**, *46*, 5670–5703.
- (25) Jiang, S. H.; Duan, G. G.; Hou, H. Q.; Greiner, A.; Agarwal, S. Novel Layer-by-Layer Procedure for Making Nylon-6 Nanofiber Reinforced High Strength, Tough, and Transparent Thermoplastic Polyurethane Composites. *ACS Appl. Mater. Interfaces* **2012**, *4*, 4366–4372.
- (26) Miao, Y. E.; Fan, W.; Chen, D.; Liu, T. X. High-Performance Supercapacitors Based on Hollow Polyaniline Nanofibers by Electrospinning. *ACS Appl. Mater. Interfaces* **2013**, *5*, 4423–8.
- (27) Huang, Y. P.; Ma, H.; Wang, S. G.; Shen, M. W.; Guo, R.; Cao, X. Y.; Zhu, M. F.; Shi, X. Y. Efficient Catalytic Reduction of Hexavalent Chromium Using Palladium Nanoparticle-Immobilized Electrospun Polymer Nanofibers. *ACS Appl. Mater. Interfaces* **2012**, *4*, 3054–3061.
- (28) Inagaki, M.; Yang, Y.; Kang, F. Carbon Nanofibers Prepared via Electrospinning. *Adv. Mater.* **2012**, *24*, 2547–66.
- (29) Ko, F.; Gogotsi, Y.; Ali, A.; Naguib, N.; Ye, H.; Yang, G. L.; Li, C.; Willis, P. Electrospinning of Continuous Carbon Nanotube-Filled Nanofiber Yarns. *Adv. Mater.* **2003**, *15*, 1161–1165.
- (30) Zhou, Z.; Lai, C.; Zhang, L.; Qian, Y.; Hou, H.; Reneker, D. H.; Fong, H. Development of Carbon Nanofibers From Aligned

Electrospun Polyacrylonitrile Nanofiber Bundles and Characterization of Their Microstructural, Electrical, and Mechanical Properties. *Polymer* **2009**, *50*, 2999–3006.

(31) Huang, J. S.; Liu, Y.; Hou, H. Q.; You, T. Y. Simultaneous Electrochemical Determination of Dopamine, Uric Acid and Ascorbic Acid Using Palladium Nanoparticle-Loaded Carbon Nanofibers Modified Electrode. *Biosens. Bioelectron.* **2008**, *24*, 632–637.

(32) Zhang, Z.; Li, X.; Wang, C.; Fu, S.; Liu, Y.; Shao, C. Polyacrylonitrile and Carbon Nanofibers with Controllable Nanoporous Structures by Electrospinning. *Macromol. Mater. Eng.* **2009**, *294*, 673–678.

(33) Pierson, H. O. *Handbook of Carbon, Graphite, Diamond and Fullerenes: Properties, Processing and Applications*; Noyes Publications: Park Ridge, NJ, 1993.

(34) Wojtysiak, S.; Walczyński, M. S.; Kudelski, A. Silver-Platinum Core-Shell Nanoparticles for Surface-Enhanced Raman Spectroscopy. *Vib. Spectrosc.* **2011**, *57*, 261–269.

(35) Chai, J.; Li, F.; Hu, Y.; Zhang, Q.; Han, D.; Niu, L. Hollow Flower-Like AuPd Alloy Nanoparticles: One Step Synthesis, Self-Assembly on Ionic Liquid-Functionalized Graphene, and Electro-oxidation of Formic Acid. *J. Mater. Chem.* **2011**, *21*, 17922–17929.

(36) Sinfelt, J. *Bimetallic Catalysts: Discoveries, Concepts and Applications*; Wiley: New York, 1983.

(37) Palanisamy, S.; Ku, S. H.; Chen, S. M. Dopamine Sensor Based on a Glassy Carbon Electrode Modified with a Reduced Graphene Oxide and Palladium Nanoparticles Composite. *Microchim. Acta* **2013**, *180*, 1037–1042.

(38) Wang, A.; Feng, J.; Li, Y.; Xi, J.; Dong, W. In-Situ Decorated Gold Nanoparticles on Polyaniline with Enhanced Electrocatalysis Toward Dopamine. *Microchim. Acta* **2010**, *171*, 431–436.

(39) Wei, M.; Sun, L.; Xie, Z.; Zhii, J.; Fujishima, A.; Einaga, Y.; Fu, D.; Wang, X.; Gu, Z. Selective Determination of Dopamine on a Boron-Doped Diamond Electrode Modified with Gold Nanoparticle/Polyelectrolyte-coated Polystyrene Colloids. *Adv. Funct. Mater.* **2008**, *18*, 1414–1421.

(40) Zhang, Y.; Lin, L.; Feng, Z.; Zhou, J.; Lin, Z. Fabrication of a PANI/Au Nanocomposite Modified Nanoelectrode for Sensitive Dopamine Nanosensor Design. *Electrochim. Acta* **2009**, *55*, 265–270.